Structural Basis for Antibody Catalysis of a Disfavored Ring Closure Reaction[†,‡]

Karl Gruber,[§,||] Bin Zhou,[§] Kendall N. Houk,[⊥] Richard A. Lerner,[§] Charles G. Shevlin,[§] and Ian A. Wilson*[,§]

Departments of Molecular Biology and Chemistry and the Skaggs Institute for Chemical Biology, The Scripps Research Institute, 10550 North Torrey Pines Road, La Jolla, California 92037, and Department of Chemistry and Biochemistry, University of California, Los Angeles, California 90095

Received January 27, 1999; Revised Manuscript Received March 31, 1999

ABSTRACT: The catalysis of disfavored chemical reactions, especially those with no known natural enzyme counterparts, is one of the most promising achievements of catalytic antibody research. Antibodies 5C8, 14B9, 17F6, and 26D9, elicited by two different transition-state analogues, catalyze disfavored endo-tet cyclization reactions of trans-epoxy alcohols, in formal violation of Baldwin's rules for ring closure. Thus far, neither chemical nor enzyme catalysis has been capable of emulating the extraordinary activity and specificity of these antibodies. X-ray structures of two complexes of Fab 5C8 with the original hapten and with an inhibitor have been determined to 2.0 Å resolution. The Fab structure has an active site that contains a putative catalytic diad, consisting of Asp^{H95} and His^{L89}, capable of general acid/base catalysis. The stabilization of a positive charge that develops along the reaction coordinate appears to be an important factor for rate enhancement and for directing the reaction along the otherwise disfavored pathway. Sequence analysis of the four catalytic antibodies, as well as four inactive antibodies that strongly bind the transition-state analogues, suggests a conserved catalytic mechanism. The occurrence of the putative base His^{L89} in all active antibodies, its absence in three out of the four analyzed inactive antibodies, and the rarity of a histidine at this position in immunoglobulins support an important catalytic role for this residue.

During the past decade, the combinatorial power of the mammalian immune system has been successfully exploited to generate *de novo* antibody catalysts (*1*). Early studies dealt with mechanistically very well understood esterase-like reactions (*2*, *3*), but more recently, a large number of catalytic antibodies have been selected that cover a wide range of chemical reactions (*4*). Structural information on how these catalytic antibodies function has become available only during the past few years (*5*−*16*).

One of the most formidable achievements in the field of catalytic antibodies is the catalysis of disfavored reactions. The use of binding energy not only to overcome the activation barrier but also to drive a chemical reaction in an otherwise generally inaccessible direction is of great significance in organic chemistry. The first example of such a transformation was the catalysis of the disfavored **6**-endo-tet cyclization reaction of trans-epoxyalcohol **1** (Figure 1) to form a tetrahydropyran **6** by antibodies 26D9 and 17F6 elicited by transition-state analogue **4** (Figure 2A) (*17*). However, in solution the formation of tetrahydrofuran **9** is favored in accordance with Baldwin's rules for ring closure reactions (Scheme 1) (*18*, *19*). Since then, a number of antibody catalysts for disfavored reactions have been reported, including catalysts for exo Diels−Alder reactions (*20*, *21*) and a syn elimination (*22*).

Hapten **4** was designed to induce an antibody capable of interacting with the critical features of the transition state. The formal charges on the *N*-oxide functionality were expected to resemble the electronic distribution of the substrate during the assumed transition state, while the conformation of the piperidinium ring should approximate the required geometry during ring closure (*17*). Although this approach was successful, it was uncertain which feature(s) of this hapten are actually responsible for the catalytic activity. One hypothesis, based on ab initio calculations (*23*), is that the important design feature of **4** is the placement of charge rather than the incorporation of the six-membered ring; cation-stabilizing group(s) in the binding site should be elicited by the *N*-oxide. Formation of oxepane **7** from **2** (Table 1), only in the presence of 26D9 (*24*), lends credence to this hypothesis, as the addition of an extra methylene in the substrate should be affected only by the hydrophobic and not by the electronic complementarity in the binding site.

An obvious way to answer the question regarding the dependency of catalytic activity on hapten structure is to redesign the hapten with subtle, but distinct, geometric or electronic changes and to compare the activity of the resulting antibodies with those derived from the *N*-oxide hapten **4**. One such modification would be to remove the piperidinium ring entirely and replace it with two alkyl groups. We elected to abandon this strategy because the presence of this ring may be responsible for providing the necessary space and proper hydrophobic environment for substrate binding. Thus, we substituted the *N*-oxide by an *N*-methyl piperidinium ion,

[†] This work was supported by NIH Grant PO1 CA27489 to I.A.W. and R.A.L. and an Erwin-Schrödinger-Auslandsstipendium Fellowship (J01278-CHE) to K.G. from the Fonds zur Förderung der wissenschaftlichen Forschung in Österreich.

[‡] The 5C8 Fab complexes with transition-state analogue haptens **4** and **5** have been deposited in the Brookhaven Protein Database with accession codes 25c8 and 35c8.

[§] The Scripps Research Institute.

[||] Present address: Institute of Physical Chemistry, KFU-Graz, A-8010 Graz, Austria.

[⊥] University of California, Los Angeles.

10.1021/bi990210s CCC: $18.00
Published on Web 05/12/1999

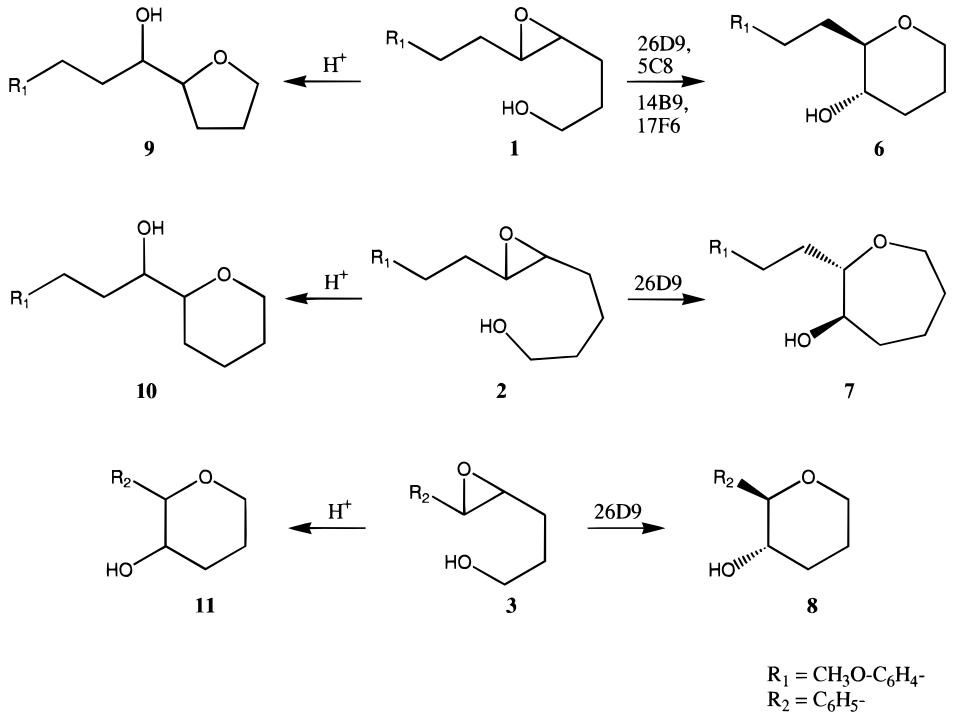

FIGURE 1: Acid-catalyzed and antibody-catalyzed reactions of epoxy-alcohols **1**−**3**.

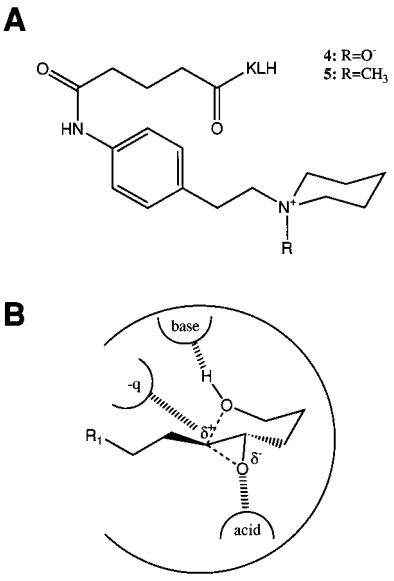

FIGURE 2: (A) Haptens used to elicit antibodies 26D9 and 17F6 (**4**), and 5C8 and 14B9 (**5**) for disfavored endo-tet reactions. (B) Expected mechanism of the ring-closure reaction.

in which a highly polarized, but neutral species is replaced by a full positive charge (hapten **5**).

In the present work, we have designed and synthesized a new hapten, *N*-methylpiperidinium **5** (*N*-methyl **5**), which led to the generation of two new antibodies, 5C8 and 14B9, both of which are capable of catalyzing the disfavored endo-tet ring closure for substrate **1**. We chose this hapten in order to probe how subtle electronic differences between haptens **4** and **5** could translate into antibodies with different catalytic properties. Antibody 5C8 has been characterized in terms of its kinetic profile and substrate selectivity and is compared here to 26D9. To elucidate the catalytic mechanism and to identify the structural basis for the observed regio- and enantiospecificity, we have determined the crystal structures

Scheme 1[a]

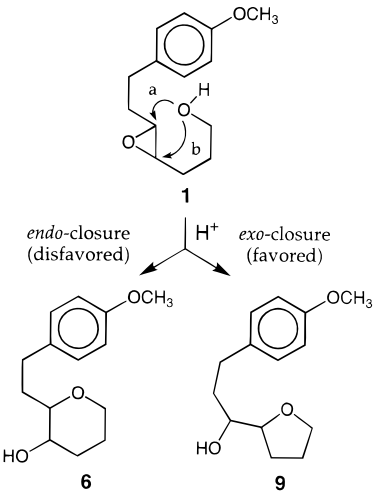

[a] In principle, closure of hydroxy-epoxide 1 can proceed via either pathway a or b (endo and exo mode, respectively). However, with this system the exo pathway is favored over the endo pathway by 97:3.

Table 1: Comparison of Antibodies 5C8 and 26D9

reaction	antibody	% endo	% ee
1 → **6**	5C8[a]	70	95
	26D9[b]	70	99
2 → **7**	5C8	no reaction	−
	26D9	>99	78
3 → **8**	5C8	*c*	0
	26D9	*c*	96

[a] 5C8 was elicited by the *N*-methyl hapten **5**. [b] 26D9 was elicited by the *N*-oxide hapten **4**. [c] Exo product not formed in background reaction.

of the newly generated Fab 5C8 in complex with both the *N*-methyl and the *N*-oxide transition-state analogues **5** and **4**. We also performed computer docking studies using ab initio calculated models of the transition states of the reaction

(*23*) and extended previous quantum-chemical studies. Sequence analysis and the comparison with mechanistically related natural enzymes suggest opportunities for improving the catalytic efficiency of these antibodies.

EXPERIMENTAL PROCEDURES

Kinetic Measurements. The kinetic parameters V_{max} and K_m were determined using an HPLC[1] assay (DAICEL chiral pak AD column with a hexane/2-propanol isocratic program of 97/3 at 1 mL/min at a wavelength of 278 nM) by measuring the initial rate of product formation. Initial rates were measured with less than 6% of the consumption of substrate. An external standard of 4-(4-methoxyphenyl)-1-butanol (20 μM) was used to calculate the amount of product formed. HPLC response factors were determined using authentic samples of both standard and product. An aliquot of antibody stock solution (50 mM PBS buffer, pH 6.8) was diluted with 50 mM PBS buffer (pH 6.8) providing 5 mL of a 2.5 μM solution of protein. Varying amounts of the appropriate stock solution of substrate, dissolved in 10% methylene chloride in acetonitrile, were added to vials containing antibody and vortexed to initiate the reactions. The total organic component of each reaction vial was maintained at 5%. Aliquots (400 μL) of the reaction mixture were removed and extracted twice with equal portions of ethyl acetate. A centrifuge was used to separate the biphasic mixture. The combined extracts were evaporated under vacuum, and the residue was diluted with 100 μL of the external standard and analyzed by HPLC. The concentrations of substrate ranged from 80 to 1000 mM, thus bracketing the K_m value.

*Synthesis of Hapten **5**.* All starting materials were purchased from the Aldrich Chemical Co. All structures of the synthesized materials were verified by ^{1}H NMR and ^{13}C NMR spectroscopy; the mass spectral data were consistent with the expected molecular weights of all compounds. Chemical shifts were recorded on a Bruker AM-300 or a Bruker AMX-500 NMR spectrometer. High-resolution mass spectra were determined using a VG ZAB-ZSE mass spectrometer under fast ion bombardment (FIB) conditions.

*[2-(4-Nitrophenyl)ethyl]piperidine (**12**).* Freshly distilled piperidine (3.8 mL, 38.4 mmol) was added to a solution of 4-nitrophenylethyl bromide in dichloromethane (4.0 g, 17.4 mmol/30 mL). The reaction mixture was refluxed for 4 h, the solvent removed under vacuum, and the residue purified by column chromatography (9:1 dichloromethane/methanol, $R_f = 0.47$), resulting in 3.74 g of product (92%).

*4-(2-Piperidylethyl)phenylamine (**13**).* Into a pressure tube were placed 80 mL of ethanol and **12** (3.7 g, 15.8 mmol) followed by 10% Pd/C (50 mg). The tube was charged with 55 psi hydrogen gas and allowed to shake for 20 min. The mixture was filtered through a plug of Celite, and stripped of solvent, yielding 3.19 g of a clear yellow oil (99%).

*4-{N-[4-(2-Piperidylethyl)phenyl]carbamoyl}butanoic Acid (**14**).* Glutaric anhydride (1.03 g, 9.03 mmol), followed by triethylamine (920 μL, 6.6 mmol) and a catalytic amount of (dimethylamino)pyridine (5 mg), were added to a solution of **13** (1.22 g, 6.0 mmol) in dichloromethane (10 mL). The solution was stirred for 16 h and the solvent removed under reduced pressure. The residue was dissolved in 1 M HCl (2 mL) and purified by reverse-phase column chromatography (30% acetonitrile/water). The fractions were combined and lyophilized yielding 2.2 g of a white powder (85% as the triflate salt).

*4-(N-{4-[2-(Methylpiperidinium)ethyl]phenyl}carbamoyl)-butanoic Acid (**5**).* To a solution of **14** (100 mg) in 50:50 methanol/water (1 mL) 120 mg of potassium carbonate and 400 μL of methyl iodide were added. The reaction mixture was allowed to stir for 16 h, and the solvent was reduced in volume under negative pressure in a fume hood. The resulting mixture was diluted with 1 mL of 0.1% aqueous trifluoroacetic acid and purified by preparative HPLC (70:30 acetonitrile/water 0.1% trifluoroacetic acid, 10 mL/min, retention time 6.8 min). The fractions were combined and lyophilized yielding 84 mg of a white powder (82% as the triflate salt).

Stereochemical Analysis of Antibody-Catalyzed Reactions: Both antipodes of epoxide **1** (trans-R,R; trans-S,S) were prepared as previously described (*17*) using methods developed by Sharpless (*25*, *26*). The HPLC system, described above, enabled enantio-separation for both starting materials and products (retention times: **1**(S,S) 31.8 min; **1**(R,R) 34.1 min; **6**(2R,3S) 23.1 min; **6**(2S,3R) 22.0 min). The enantioselectivity of 5C8 was determined by incubating each optically pure isomer of **1** with 5C8 for a period of 4 h. The reaction mixtures were worked up and analyzed, as described above. To elucidate the stereochemistry of antibody-catalyzed product **6**, [**6**(2R, 3S) versus **6**(2S, 3S)], we incubated a pure sample of **1**(S,S) with 5C8 for 6 h, and **6** was collected on repeated runs until 3 mg of material was recovered. This sample was analyzed using NOESY (Nuclear Overhauser Effect Spectroscopy) and subsequently determined to be **6**(2R,3S).

Purification, Crystallization, Data Collection, and Refinement. Fab 5C8 was produced by partial enzymatic digestion of the intact IgG using 2% mercuripapain, activated by incubating with 10−20 mM cysteine and 2.5 mM EDTA (*27*) and purified using a combination of protein A and protein G affinity chromatography (*28*). All crystals were grown from a 16 mg/mL protein solution in 0.1M sodium acetate buffer, pH 5.5, at 22.5 °C using 14% PEG10K in 0.2 M Tris-malate, pH 5.5, as precipitant. The ligand was added in a molar ratio of approximately 10:1 to the Fab solution. Both data sets were collected from flash-cooled crystals (cryoprotected with 25−30% glycerol) at the Stanford Synchrotron Radiation Laboratory (SSRL, beamlines 7−1 and 9−1) using MAR image plate detectors. Data were processed to 2.0 Å resolution and scaled with DENZO and SCALEPACK (*29*). Amplitudes were calculated with TRUNCATE (*30*). The structure of the *N*-methyl complex of **5** was determined by molecular replacement using AMORE (*31*) with the partially refined structure of the unliganded Fab 5C8 (*32*) as a search model. Clear electron density, consistent with the chemical structure of **5**, was observed in the binding site of the antibody. For the complex with **4**, rigid body refinement using the Fab of the *N*-methyl complex was sufficient as a starting model. Again, the ligand could be easily built into unambiguous difference electron density.

[1] Abbreviations: Fab, antigen-binding fragment of an antibody; IgG, mouse immunoglobulin G; V_L, V_H, variable light and heavy chains; C_L, C_H1, constant light and heavy chains; EDTA, ethylenediaminetetraacetic acid; PEG, poly(ethylene glycol); vdw, van der Waals; HPLC, high performance liquid chromatography; BSA, bovine serum albumin; CDR, complementarity determining region; KLH, keyhole limpet hemocyanin.

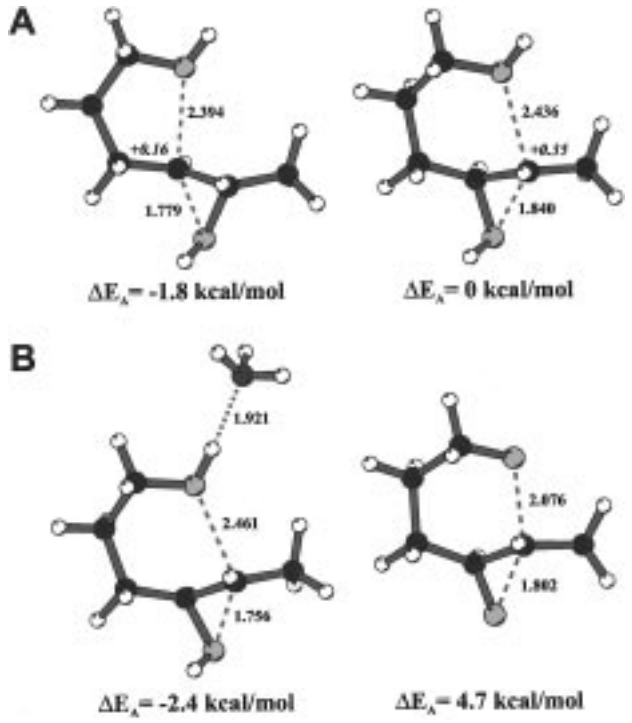

FIGURE 3: Transition states plus relative activation energies for the (A) acid-catalyzed **5**-exo (left) and **6**-endo (right) reactions and two base-promoted transformations (B). Energies were calculated using Gaussian 94 (*55*) as zero-point corrected differences between the transition states and the respective substrates at the MP2/6-31G*//HF/6-31G* level of theory. The molecular drawings were prepared using Molscript (*73*).

Both models were refined using X-PLOR (online) version 3.851 (*33*) employing the Engh & Huber set of parameters (*34*). After each round of positional and restrained *B* factor refinement, the model was checked for its fit to σ_A-weighted $2F_o - F_c$ maps (*35*), shake-omit maps [calculated using X-PLOR with about 5% of the model omitted, after adding random errors to the coordinates with an rms deviation of 0.25 Å (*36*)], and σ_A-weighted Bhat-omit maps (*37*, *38*) using O (*39*). For some loop regions, simulated annealing omit-maps (*40*) were calculated. In the later stages of refinement, the program OOPS (*39*) was used to highlight regions in the structure most likely to need rebuilding. Anisotropic scaling tensors and bulk solvent correction (*41*) were applied to the data. The Fab molecules are numbered according to standard Kabat convention (*42*) with light (L) and heavy (H) chain identifiers. For both structures, contiguous electron density was observed for the whole polypeptide chain, except for a disordered loop in the C_H1 domain, consisting of residues H128−H136, as observed in almost all other Fab structures [for example, see ref *43*]. This region was included in the refinement with zero occupancy, but excluded from subsequent structure analyses. Structure validation was carried out with PROCHECK v3.3 (*44*). Both models are of good stereochemical quality with 88.7% (complex with **5**) and 89.3% (complex with **4**) of the residues in the most favored regions of the Ramachandran plot. Only one residue (Thr^{L51}) was found in a disfavored region in both structures (mean $\phi = 71.4°$, mean $\varphi = 50.1°$), but it is in a tight γ-turn, as commonly observed in other antibody structures (*45*).

Theoretical Calculations. The calculated transition-state structures (Figure 3A) were extended by a benzyl group, and the proton at the epoxide was removed. Charges on the transition-state atoms were obtained with semiempirical AM1 calculations (*46*). The protonation states of active site residues were deduced from their environment in the crystal structures, with Asp^{H95} protonated and Asp^{H101} and His^{L89} unprotonated. Simulated annealing with AutoDock (*47*, *48*) was used to locate low-energy binding modes. From 120 different, randomly generated initial structures, the position and orientation of the ligand and the three dihedral angles in the two-methylene linker between the phenyl ring and the epoxide were allowed to vary, while the antibody structure was held fixed in the X-ray geometry. Each simulation involved 200 cycles of simulated annealing. The energy of interaction was calculated using a potential function composed of van der Waals and Coulombic terms. As a validation of this procedure, both transition-state analogues **4** and **5** were docked (*47*, *48*) into the antibody (Asp^{H95} was unprotonated for the docking of **4** and protonated for the docking of **5**), and the binding positions reproduced the experimental ones with an rms deviation of 0.3−0.5 Å. Molecular surfaces were calculated using the program MS (*49*), with a probe radius of 1.7 Å and standard vdw radii (*50*).

Scheme 2: Synthesis of Hapten **5**[a]

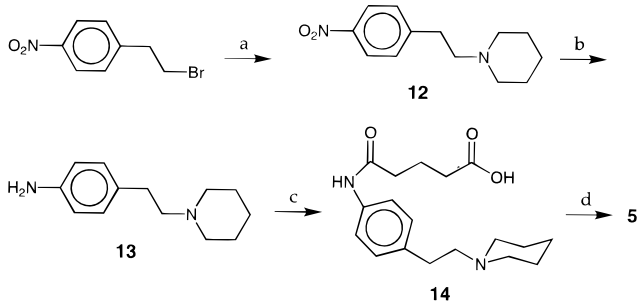

[a] Conditions: (a) piperidine, 45 °C, 4 h, 92%; (b) Pd/C, H_2, methanol, 99%; (c) glutaric anhydride, 85%; (d) MeI, K_2CO_3/MeOH/H_2O, 82%.

HPLC Analysis. An Hitachi L-6200 liquid chromatogram equipped with a UV detector was employed. We used a DAICEL chiral pak AD with a hexane/2-propanol isocratic program of 97/3, a flow rate of 1 mL/min, and a wavelength of 278 nm.

RESULTS AND DISCUSSION

Hapten **5** was synthesized (Scheme 2), coupled to keyhole limpet hemocyanin (KLH), and used to immunize 129GIX+ mice (*51*). Twenty-one of the resulting monoclonal antibodies were shown by enzyme-linked immunosorbant assay (ELISA) to bind to the BSA conjugate of **5** (*52*) and were screened against epoxy-alcohol **1** for the formation of **6** using a normal phase chiral HPLC column. Two of these antibodies, 5C8 and 14B9, were regioselective catalysts for the formation of **6**, but antibody 5C8 was more efficient and stereoselective than 14B9 and produced about 70% of (2R, 3S)-**6** in 95% enantiomeric excess (Table 1). When a racemic mixture of **1** is incubated with 5C8, both enantiomers of **1** are utilized in the antibody-catalyzed reaction but give rise to different product distributions. In both cases, 5C8 enhances the formation of the exo product. For the SS-enantiomer, formation of the disfavored endo product was also enhanced, whereas for the RR-enantiomer, the ratio between exo and endo product was only slightly altered from the uncatalyzed reaction in solution. If **1** is allowed to react to completion,

the ratio of **9** to **6** is 97:3. Formation of (2R, 3S)-**6** with 5C8 follows Michaelis−Menten kinetics, with $K_m = 595\ \mu M$ and $k_{cat} = 1.7\ min^{-1}$ at pH 6.8 (compared to $K_m = 356\ \mu M$ and $k_{cat} = 0.91\ min^{-1}$ for 26D9) and is inhibited with stoichiometric quantities of its original hapten **5** and the *N*-oxide **4**. Comparison of k_{cat}/k_{uncat} is not possible because formation of the disfavored endo product **6** in the uncatalyzed reaction was negligible under our assay conditions (*17*).

A comparison of the activities of 5C8 and 26D9 is summarized in Table 1. The regioselectivities of both 5C8 and 26D9 for **1** are remarkably similar. Both antibodies also exhibit high enantioselectivities for this substrate [favoring the formation of (2R,3S)-**6**] and possess similar kinetic profiles. Differences between the two antibodies, however, became evident in the transformation of **3**, for which no exo product is observed in solution, and is probably due to the incipient benzylic-stabilized carbocation of **3**, as proposed for the analogous allyl epoxides (*53*). While formation of **8** is catalyzed by 5C8, this antibody, unlike 26D9, does not show a preference for the choice of enantiomer of **3**. Furthermore, 26D9 provides excellent regio- and enantioselectivities for the intramolecular closure of **2** to form the oxepan **7** (*24*), whereas no catalysis is observed with 5C8.

Mechanistic Possibilities. At least two possible pathways are conceivable for the reaction, irrespective of the size of the ring that is formed. The first pathway consists of a single, intramolecular S_N2-type reaction that inverts the absolute configuration at the reaction center, whereas the second involves nucleophilic attack by a protein residue via a covalent intermediate. This intermediate must then be cleaved by a second, intramolecular nucleophilic attack of the alcohol group in order to release the product. In this case, two consecutive inverting substitutions would most likely leave the net absolute configuration unchanged. Since all four antibodies catalyze the ring closure with inversion about the epoxide carbon atom, a mechanism similar to the first, one-step transformation seems more likely.

It can further be anticipated that an acidic residue in the binding site would protonate the leaving oxygen atom, while a base close to the alcohol group would facilitate the reaction by increasing the nucleophilicity of this group (Figure 2B). Finally, a strategically positioned, negative charge could stabilize the partial positive charge that develops at either oxirane carbon atom in the transition state (*54*).

Ab initio calculations (*23*) of the transition states for the acid-catalyzed transformations of trans-4,5-epoxyhexan-1-ol (a model for **1**) have predicted a higher S_N1 character of the **6**-endo transition state, as indicated by an increased partial charge on the respective epoxide carbon atom and longer distances for both the nucleophile and the leaving group from this center (Figure 3A). The calculated difference in activation energy (1.8 kcal/mol in favor of the **5**-exo transformation) is also in good agreement with the observed ratio of exo to endo product in solution.

To assess the importance of a base in activation of the nucleophile, we carried out additional gas phase quantum-chemical calculations on this system that involved an ammonia molecule hydrogen-bonded to the alcohol, as well as to the fully deprotonated alkoxide. The geometries of the reactants and the respective transition states were optimized at the HF/6-31G* level of theory using Gaussian 94 (*55*). Single-point energies at these stationary points were calculated using second-order Möller−Plesset perturbation theory (MP2). In the reactants, the hydrogen bond between ammonia and the alcohol group stabilizes the complex by 18.1 kcal/mol. This stabilization increases to 20.5 kcal/mol in the transition state and results in a 2.4 kcal/mol decrease in the activation energy compared to the acid-catalyzed reaction (Figure 3B). Since the calculations were carried out in the gas phase, the strength of the ionic hydrogen bonding is very large. The complexation with ammonia had only minor effects on the energy difference between the **6**-endo (1.8 kcal/mol) and the **5**-exo (1.4 kcal/mol) transition states.

While protonation of the epoxide results from an ultimate acid catalyst, a fully deprotonated alcohol group similarly represents the extreme of specific base catalysis. As expected, the increased nucleophilicity of the alkoxide and the unprotonated epoxide oxygen, being a rather poor leaving group, led to a very compact, S_N2-like, transition state. The activation barrier for this reaction was calculated to be higher by 4.7 kcal/mol in the case of the **6**-endo reaction (Figure 3B). These results indicate that base promotion can have a positive influence on the reaction rate, but more importantly, protonation of the epoxide makes the oxygen a better leaving group.

Table 2: Data Collection and Refinement Statistics

	Fab 5C8 + *N*-methyl (**5**)	Fab 5C8 + *N*-oxide(**4**)
space group	C2	C2
unit cell dimensions	$a = 112.0$ Å	$a = 111.2$ Å
	$b = 80.0$ Å	$b = 79.9$ Å
	$c = 64.9$ Å	$c = 65.0$ Å
	$\beta = 118.0°$	$\beta = 118.2°$
temperature	−176 °C	−176 °C
resolution	25.0−2.0 Å	50.0−2.0 Å
(outer resolution shell)	(2.03−2.00 Å)	(2.03−2.00 Å)
no. of observations	231 822	249 541
unique reflections	33 080	33 264
completeness	96.7% (93.4%)[a]	98.0% (97.6%)
mean I/σ_I	16.9 (2.9)	20.0 (3.2)
R_{sym}	0.057 (0.304)	0.065 (0.387)
% $F > 2\sigma_F$	92.6 (75.3)	93.1 (80.8)
no. of protein atoms	3251	3251
solvent (H_2O)	232	312
ligand	24	24
R_{cryst}[b]	0.229 (0.215)	0.206 (0.198)
R_{free}[b,c]	0.292 (0.276)	0.261 (0.251)
rms deviations[d]		
bond lengths	0.007 Å	0.009 Å
bond angles	1.4°	1.5°
dihedrals	30°	30°
improper dihedrals	0.7°	0.7°
B values (RS-corr)[e]		
protein	40 Å^2 (0.88)	24 Å^2 (0.92)
solvent	43 Å^2 (0.79)	31 Å^2 (0.85)
ligand	26 Å^2 (0.94)	21 Å^2 (0.87)

[a] Values for highest-resolution shell are given in parentheses. [b] All data ($F > 2\sigma_F$). [c] 7.5% of the data were set aside for the R_{free} calculation during the entire refinement. [d] Compared to the Engh & Huber set of parameters. [e] Real space correlation (calculated using O) for σ_A-weighted $2F_o - F_c$ maps.

Structure Analysis. The crystal structures of Fab 5C8 in complex with transition-state analogues **4** and **5** were both determined at 2.0 Å resolution (Table 2). Both structures are of good quality, consistent with the resolution of the diffraction data. The overall antibody structures are similar to those reported for other Fabs (*56*). The antigen-binding site is located at the apex of the variable domains (Figure 4)

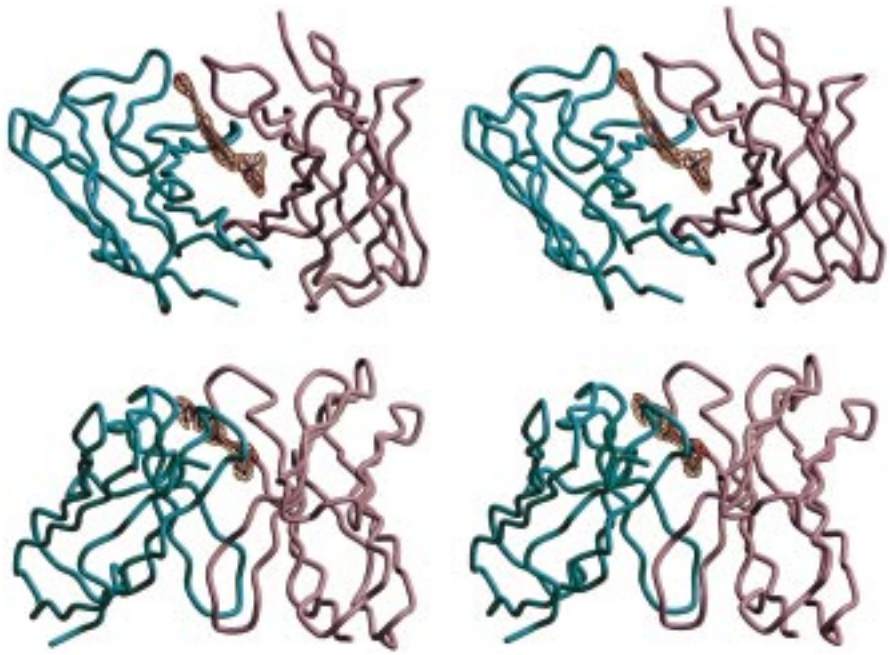

FIGURE 4: Stereoview of catalytic antibody Fab 5C8 in complex with transition-state analogue **5** viewed from above (top) and from the side (bottom) of the variable domain. The variable light chain (left, light-blue), the variable heavy chain (right, pink), and **5** are shown together with the shake-omit electron density map ($F_o - F_c$) for the ligand, contoured at 3σ. The electron density was calculated and contoured using XtalView (*36*). Figures 4−7 were prepared using Molscript (*73*) and Raster3D (*74*, *75*).

in a pocket formed by the six hypervariable loops (L1-L3 of the light chain and H1-H3 of the heavy chain), called CDR's (complementarity determining regions).

In both structures, the ligand adopts an extended conformation and lies in an elongated narrow cleft, which is closed on one side. The orientation of the ligands is such that their piperidinium rings face inward, where they are totally shielded from solvent, while the glutaric acid chains run almost parallel to the CDR-H3 loop and are partially solvent accessible. This orientation is consistent with the terminal carboxylate being linked to the carrier protein (KLH) in the immunization procedure.

The most prominent feature of compound **5** is the positive charge of the quaternary piperidinium ring. The binding site of the antibody has adapted to this feature and contains two aspartic acid residues (H95 and H101) that bind the ligand like a pair of tweezers (Figure 5A). The distances of the nearest carboxylate oxygens of the two Asp residues to the quaternary nitrogen are 3.7 Å (H95) and 4.0 Å (H101). The two aspartate side chains themselves are held in place by hydrogen bonds with Tyr^{L91} and His^{H35} (in the case of Asp^{H95}) and Tyr^{L36} and Trp^{H103} (for Asp^{H101}). Besides this electrostatic complementarity, antigen recognition is mediated mostly by van der Waals interactions. The benzene moiety of the ligand is sandwiched between His^{L34} (with the two rings being almost parallel) and Pro^{H96} (via Cγ and Cδ). The hydrocarbon part of the piperidinium ring is bound in a mostly hydrophobic pocket built up from residues His^{L89}, Tyr^{L91} (both L3), His^{H35} (H1), Phe^{L98}, Val^{H37}, Trp^{H47}, Ala^{H93}, and Trp^{H103} [all framework residues as defined by ref *42*].

Compounds **4** and **5** are similar except for the full positive charge in **5** being replaced by a polarized N−O bond in **4**. Superposition of the main-chain atoms of the central β-sheets of the Fab variable domains reveals only minor conformational and positional differences of the two ligands (rms deviation: 0.49 Å). In both structures, the piperidinium ring adopts the favored chair conformation with the methyl group or the oxygen in an axial position. In the complex with **4**, however, the whole ring is tilted by about 20° so that the oxygen atom approaches the carboxylic group of Asp^{H95} (Figure 5B). The close contact between Asp^{H95} and the *N*-oxide of the ligand (2.6 Å) requires one of the two (most likely Asp^{H95}) to be protonated at the pH of crystallization (5.5). The conformation of the glutaric acid linker varies slightly in the two structures with torsion angle differences of about 20 to 40°.

Despite the conformational differences between the ligands, the pattern of binding interactions (especially the vdw contacts) is very similar. The number of contacts is almost equally distributed among the heavy and light chains. The greatest number of contacts occurs between ligand and CDR-H3, while CDR-L2 and CDR-H2 are not involved at all in ligand binding. In both structures, more than 90% of the solvent accessible surface of the ligand is buried upon complex formation. Only about 60% of the total protein surface buried in the complex involves atoms from the CDR loops. The extensive use of framework residues for hapten binding is due to deep penetration of the ligands within the Fab combining site (Figures 4 and 6). In contrast, the framework contribution to ligand binding in other Fab-antigen complexes is generally less than 10% (*57*).

The Fab component of the two complex structures is also essentially unaffected by the slight ligand-binding differences. The elbow angles, defined as the angle between the pseudo-2-fold rotation axes relating V_L to V_H and C_L to C_H1, are 167.0° (for **4**) and 168.2° (for **5**). For the Fab variable domain, the rms deviation calculated for backbone atoms, after superimposing the central β-sheets is 0.24 Å. The five CDR loops L1, L2, L3, H1, and H2 adopt conformations close to their expected canonical loop conformations, as

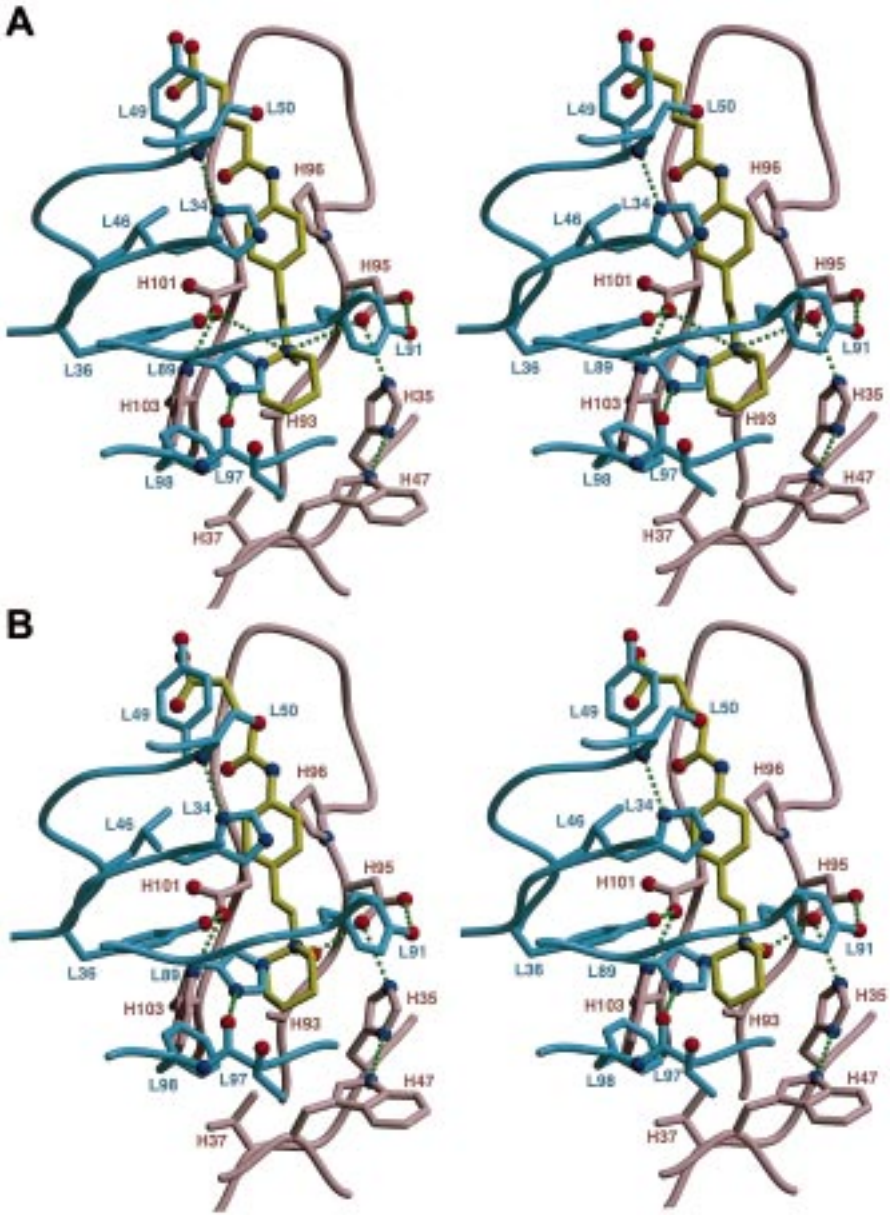

FIGURE 5: Stereoview of the antibody combining site in the structures with **5** (A) and **4** (B). The light chain is drawn in light-blue, the heavy chain in pink. Bonds in the ligand are yellow; nitrogen and oxygen atoms are shown as blue (N) and red (O) spheres. Hydrogen bonds and the interactions of Asp^{H95} and Asp^{H101} with the quaternary nitrogen of **5** are indicated by small green spheres.

defined for immunoglobulin structures (*58*). With the exception of CDR-H2 (rmsd. 0.45 Å), the CDR loops are mostly unaffected by the different ligands with backbone rms deviations in the range of 0.14−0.26 Å for the two structures. The CDR-H2 deviation is mostly associated with conformational changes of the backbone around residues Gln^{H64} and Gly^{H65}, although neither of these residues is in direct contact with the ligand.

Catalytic Mechanism. A number of residues are potentially capable of acting as an acid or base in the active site of antibody 5C8 (Figure 5): two aspartic acids (H95 and H101), three histidines (L34, L89, and H35), and two tyrosines (L36 and L91). Their ability to perform such a role relies on their respective pK_a values. Due to close contacts with the *N*-methyl group of **5** and the oxygen of **4**, Asp^{H95} is most likely unprotonated in the first complex and protonated in the second, suggesting that its pK_a is shifted toward a value above 5. Asp^{H101} accepts a hydrogen bond from Tyr^{L36} and is partially solvent exposed. Its pK_a would then be essentially normal and Asp^{H101} would be charged in both structures. His^{L34} accepts a hydrogen bond from the main-chain amide of Ser^{L50} (3.0 Å). Similarly, His^{H35} accepts a hydrogen bond from the indole NHϵ1 of Trp^{H47} (3.0 Å), indicating that both residues are neutral in the conformation observed in the crystal structures. His^{L89}, on the other hand, donates a hydrogen bond (via NHδ1, 2.9 Å) to the main-chain carbonyl of Thr^{L97} (Figure 5). With the imidazole Nϵ2 not involved in any close contacts, this residue has the possibility of being charged or uncharged. The binding site otherwise is rather hydrophobic, except for these two aspartic acids that could stabilize the imidazolium ion. A positively charged side chain, on the other hand, would not be very well suited for binding the positively charged transition-state analogue **5**. Thus, the pK_a of His^{L89} must be shifted to lower values with the side chain unprotonated in both structures. Since both tyrosine residues in the binding site (Tyr^{L36} and Tyr^{L91}) have

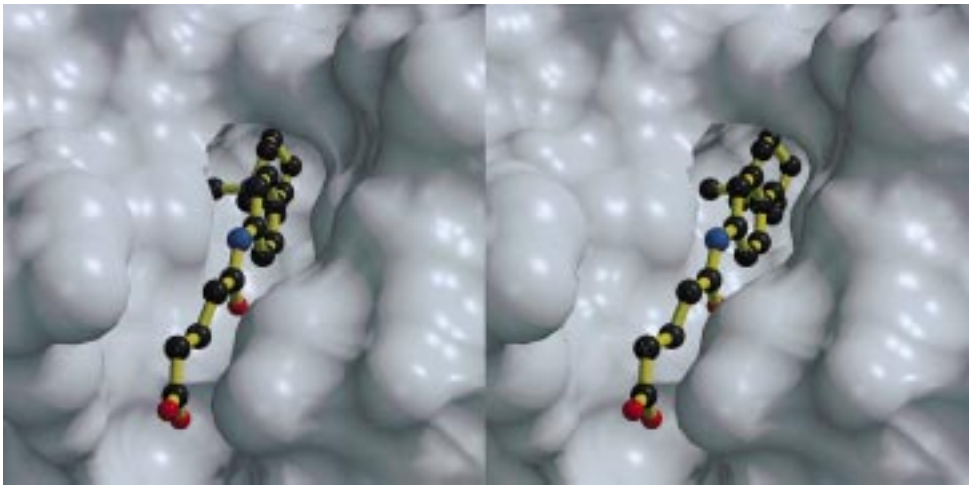

FIGURE 6: Surface representation of Fab 5C8 looking into the binding site. The ligand (**5**) is shown with yellow bonds and black (C), blue (N), and red (O) spheres representing the atoms.

their hydroxyl groups within hydrogen bonding distance to either Asp^{H95} or Asp^{H101}, they should both be protonated.

To investigate the catalytic mechanism, we docked the ab initio models of all four possible transition states into the binding site of the antibody using the program AutoDock v2.4 (*47*, *48*). In each case, the docked structure with the lowest energy was subject to a molecular mechanics minimization employing the Merck Molecular Force Field (MMFF) as implemented in Spartan (SPARTAN, version 5.0, Wavefunction, Inc., Irvine, CA, 1997), allowing the same degrees of freedom as in the docking calculations (*47*, *48*). This procedure gave an overall orientation of the ligands that differs only slightly from the crystal structures. The resulting models of the protein transition-state complexes for the **6**-endo transformations are shown in Figure 7. Essentially the same protein−ligand interactions were observed for the respective **5**-exo transition states.

As expected, the epoxide oxygen is positioned close to Oδ1 of Asp^{H95} (approximately 2.5 Å) in both cases. The alcohol groups lie between His^{L89} and Tyr^{L36}. In the case of the SS-enantiomer, the hydroxyl group is closer to His^{L89} than to Tyr^{L36} (2.7 Å vs 4.0 Å, Figure 7A), suggesting that the former residue is the base anticipated in the active site (Figure 8A). Without allowing conformational changes of active site residues, however, the interaction geometry is not perfect for proton transfer with the alcohol group approaching the imidazole ring face-on. The transformation of the RR-enantiomer, on the other hand, seems to involve the diad Tyr^{L36}−Asp^{H101} as the base (Figures 7B and 8B). The distance between the two hydroxyl groups was found to be 2.6 Å compared to 3.2 Å between the alcohol and His^{L89}. Although only speculations about the pK_a values of this hydrogen-bonded network can be made, it is conceivable that Tyr^{L36} could accept the proton and itself protonate Asp^{H101}. In both cases, the two other histidine residues in the binding site are too distant from the reacting groups and their imidazole rings are incapable of accepting an additional proton at physiological pH (see above).

Although slight geometric differences between the **5**-exo and **6**-endo transition states may, in principle, be exploited for driving the reaction in a certain direction, charge stabilization seems to be the best explanation for the observed differentiation of the two pathways. In the design of haptens **4** and **5**, the main emphasis was focused on providing a (partial) positive charge on the nitrogen in order to mimic the increased positive charge at the central carbon atom in the **6**-endo transition state and, hence, to elicit a stabilizing, complementary negative charge in the antibody combining site (*17*). The position of this charge within the hapten is crucial and was suggested to be the most important constituent of the transition-state analogue design (*54*). The most likely candidate in the binding site of 5C8 for charge stabilization is Asp^{H101}. Utilization of this residue as a proton acceptor, however, might impair its ability to stabilize the **6**-endo transition state.

The discussion of the enantiospecificity is complicated by the fact that the transformations of both enantiomers of **1** are catalyzed to some extent by the antibody 5C8, which appears to lower the reaction barrier for both enantiomers and both pathways. Only in the case of the SS-enantiomer is the difference in activation energy between the exo and endo pathways altered significantly from the situation in solution, resulting in a 95% enantiomeric excess for the formation of (2R,3S)-**6** (Table 1). In view of the assumed similar interactions of both enantiomers of the transition state with the antibody (Figure 7), very subtle stereoelectronic effects are expected to be responsible for the observed specificity. One possible explanation might be the putative utilization of Tyr^{L36}−Asp^{H101} as the base in the transformation of the RR-enantiomer that could weaken the ability of the binding site to stabilize the positive charge in the transition state and, therefore, lead to reduced formation of (2S,3R)-**6**.

Our favored mechanism that is consistent with the available structural information and the observed product distribution employs general acid/base catalysis with Asp^{H95} as the acid to open the oxirane ring and His^{L89} as the base to promote the nucleophilic attack of the alcohol group (Figure 8A). An alternative mechanism involving Tyr^{L36}−Asp^{H101}, instead of His^{L89}, is more likely only for the transformation of the RR-enantiomer (Figure 8B).

Sequence Comparisons. Genes for the variable domains of four antibodies (5C8, 14B9, 17F6, and 26D9) capable of catalyzing the disfavored **6**-endo ring closure reaction were cloned and sequenced according to the previously established method (*59*). Antibodies 5C8 and 14B9, elicited by the same

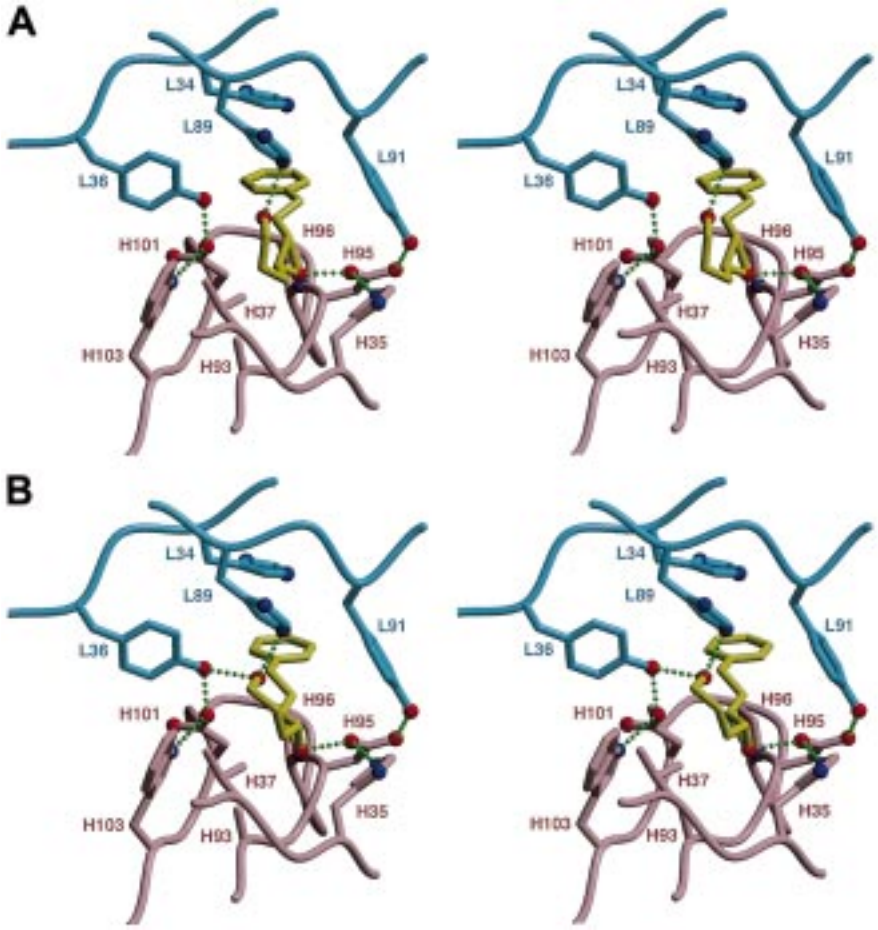

FIGURE 7: Stereoview of the modeled complexes of 5C8 and the SS- (A) and RR-enantiomer (B) of the **6**-endo transition state. The light chain is drawn in light-blue, the heavy chain in pink. Bonds in the transition-state models are yellow; nitrogen and oxygen atoms are shown as blue (N) and red (O) spheres. Hydrogen bonds are indicated using small green spheres. The view is approximately perpendicular to the one in Figure 5.

hapten (**5**), have very similar primary structures with more than 80% identical residues in their variable domains. Almost all ligand-contacting residues are the same in both sequences. Most importantly, the putative catalytic residues Asp^{H95} and His^{L89} (as well as Asp^{H101} and Tyr^{L36}) are conserved. Mutations of contact residues are found in the middle of the CDR-H3 loop, which interacts only with the glutaric acid linker that is replaced by the much smaller methoxy group in the substrate (Figure 1). The only mutation involving a side-chain contact to the piperidinium ring of the ligand is Ala^{H93} to valine in 14B9. This residue is positioned below the piperidinium ring with its Cβ pointing up (Figure 5). As antibody 14B9 is less efficient than 5C8, the larger Val^{H93} side chain probably interferes with substrate binding.

Antibodies 26D9 and 17F6, on the other hand, show some very interesting differences in their amino acid sequences. Their light chains are highly homologous to 5C8 and 14B9 (>80% identity), whereas significant changes are observed in the heavy chains with only around 50% identity. In both cases, residue Asp^{H95} is mutated to a tyrosine. At the same time, its hydrogen-bonding partner, His^{L35} is replaced by a serine, presumably allowing for accommodation of the larger tyrosine side chain. However, the second aspartic acid Asp^{H101} and the potential bases His^{L89} and Tyr^{L36} are conserved. Another difference is Ala^{H93} to threonine, which could potentially hydrogen bond to the *N*-oxide (**4**) in 26D9 and 17F6. All other residues that form the hydrophobic pocket, which accommodates the hydrocarbon part of the piperidinium ring, are conserved or highly homologous.

From this sequence analysis, it appears that all four antibodies bind the piperidinium moiety of their respective haptens in a similar fashion. Also, the catalytic mechanism derived for 5C8 appears to be applicable to these other antibodies, particularly for 14B9, since all key residues are conserved. Antibodies 26D9 and 17F6 show considerable sequence differences but may catalyze the reaction in an analogous way. The role of the acid in 5C8 could in principle be taken over by Tyr^{H95}, with the resulting phenolate ion being stabilized by a hydrogen bond from Ser^{H35}. All three residues that are potentially involved in activating the alcohol group (Tyr^{L36}, His^{L89}, and Asp^{H101}) are conserved and could act similarly. The mutation Ala^{H93} to threonine may even be an advantage, because a hydrogen bond donated by this residue may be able to stabilize further the partial negative charge that develops on the leaving oxygen.

Some of the residues in the binding site of these antibodies are highly conserved among murine immunoglobulins, while others vary considerably. At position H95, aspartic acid is the most common residue (20%), although this position is very variable and has accommodated all 20 amino acids at least once with a 2% occurrence of tyrosine (*60*). Also, Tyr^{L36} (84%) and Asp^{H101} (88%) are the most frequent residues at

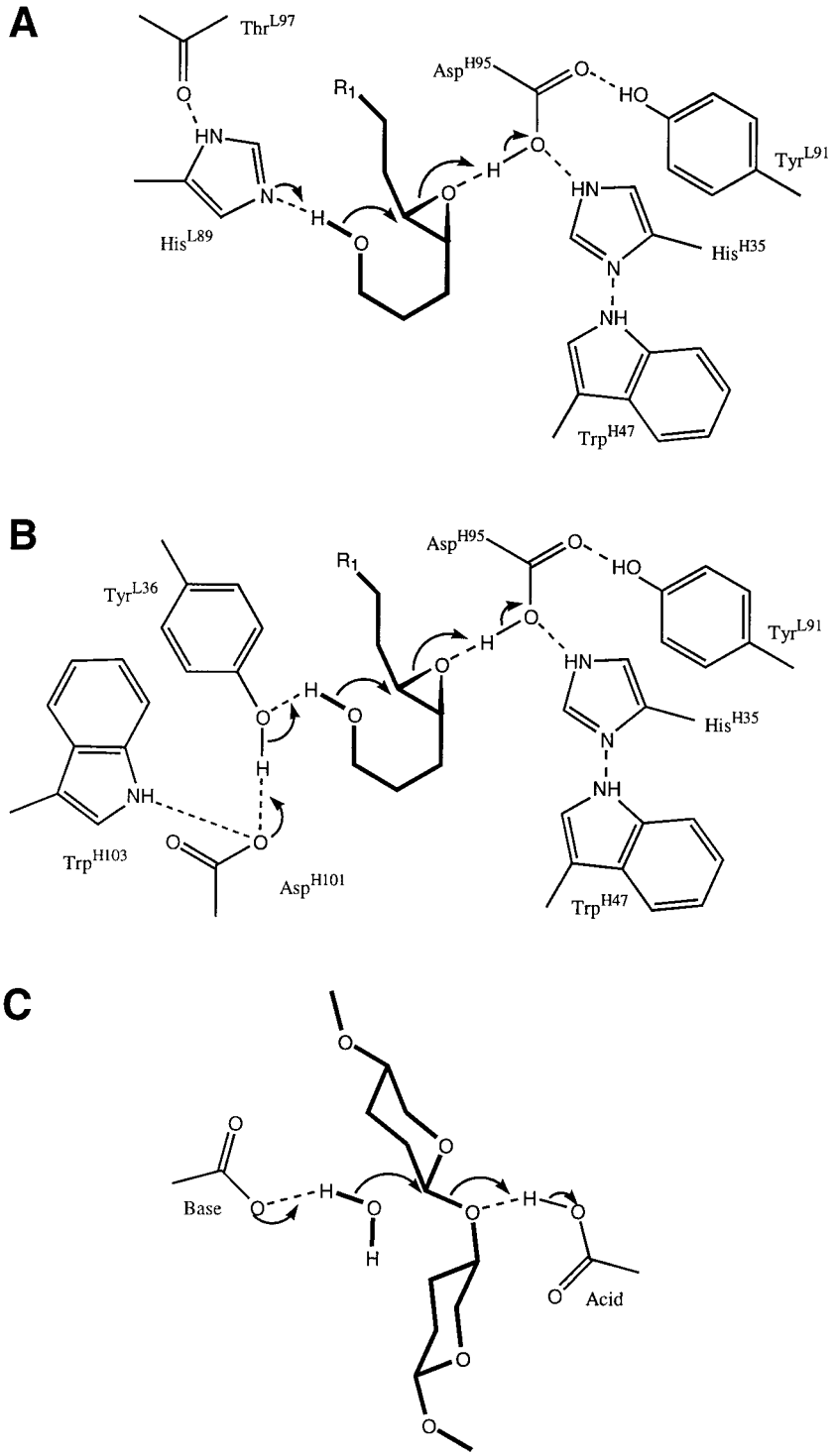

FIGURE 8: Proposed catalytic mechanism of antibody 5C8 with Asp^{H95} as the acid that opens the oxirane and His^{L89} (A) or Tyr^{L36}-Asp^{H101} (B) as the base that activates the alcohol group. Hydrogen bonds to other active site residues are shown. (C) Possible mechanism of "inverting" glycosidases.

these positions. The most common residue at position L89 is glutamine (62%), while histidine is present in only 5% of all murine κ-light chains sequenced to date (*60*).

In an effort to assess the importance of the putative active site residues, we also determined the primary structures of four antibodies that were elicited by the same *N*-methyl hapten (**5**) and showed strong binding of the transition-state analogue but no catalytic activity (Figure 9). The first major difference was found to be the absence of His^{L89} in three of the four inactive antibodies; 3B2 does have a histidine at this position and the putative diad Tyr^{L36}−Asp^{H101}. However, its inactivity may be explained by the occurrence of three additional aspartate residues in the central region of the CDR-H3 loop. Therefore, the hapten and the substrate may be bound in a different way that prevents them from interacting with His^{L89} and Tyr^{L36}−Asp^{H101}. The same pattern was also found in 1A11, the heavy chain of which is almost identical to 3B2. In 7D2, the positive charge of the quaternary nitrogen is most likely bound by negatively charged residues on CDR-L3 (two aspartates, one glutamate) rather than by CDR-H3.

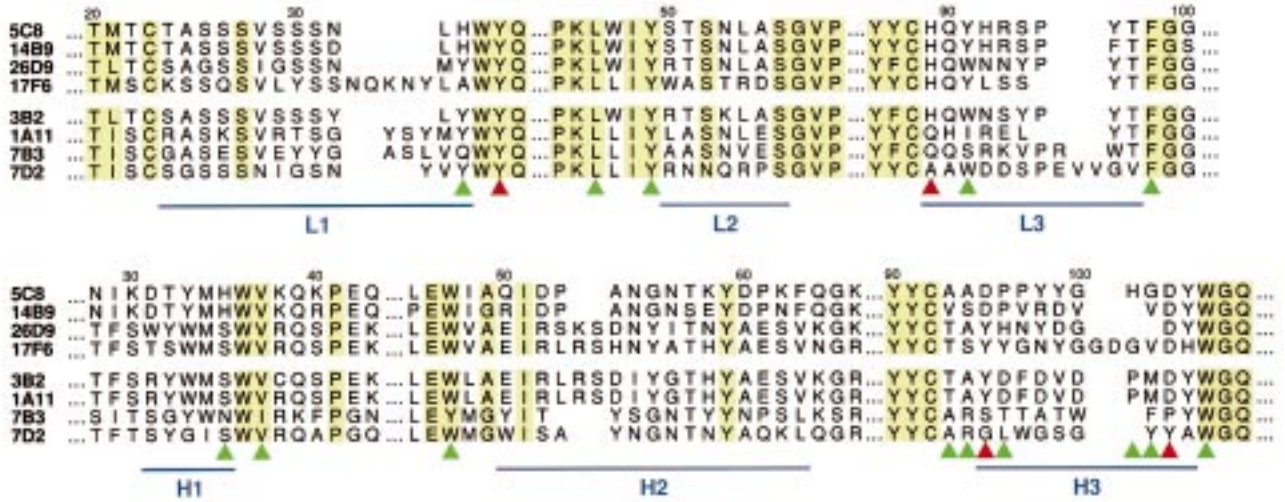

FIGURE 9: Sequence alignment of the hypervariable regions of the light (top) and heavy chains (bottom) for four active (5C8, 14B9, 26D9, and 17F6) and four inactive antibodies (3B2, 1A11, 7B3, and 7D2) that were all elicited by hapten **5**. Sites with an AMAS-score (*76*) of greater than or equal to 9 (identical or highly homologous based on physicochemical criteria) are shaded in yellow. Residues that contact the ligand in the 5C8 complex structures are marked with triangles. Red triangles are used to mark residues that are presumably important for catalysis. The alignment was performed using Clustal W (*77*). The figure was prepared using Alscript (*78*).

A completely different mode of binding is expected for 7B3, since no negatively charged residues are present in CDR-L3 or CDR-H3. Taken together, the occurrence of the rather rare His^{L89} in all catalytically active antibodies and its absence in most of the inactive ones are indicators for its presumed importance in the catalytic mechanism and support our proposed mechanism (Figure 8A).

Comparison with Natural Enzymes. We are not aware of any natural enzymes that catalyze the same reaction as these antibodies. The brevotoxins and other related polyether natural products were thought to be formed via a series of disfavored enzyme-catalyzed hydroxy-epoxide ring closures. Several research groups were unsuccessful in their search for this putative enzyme class (*61*−*64*), which included the synthesis of, and subsequent screening with, logical epoxide precursors (*65*−*68*). However, a number of enzymes do utilize epoxides as substrates. The reactions that are catalyzed range from very complex terpenoid cyclizations to comparatively simple epoxide hydrolysis reactions, the latter being more closely related to the antibody-catalyzed reaction. Among these hydrolases, mammalian soluble and microsomal epoxide hydrolases, which are involved in the detoxication of potentially harmful xenobiotic epoxides, have been characterized (*69*, *70*). Their mechanism involves a covalent α-hydroxy-ester intermediate formed by a carboxylate side chain of the enzyme (*71*). This intermediate is thought to be cleaved by a base-activated water molecule attacking at the carboxyl-carbon atom of the ester and subsequent release of the diol product (*69*, *70*). This particular mechanism cannot be applied for an intramolecular cyclization reaction, simply because no product would be released by a nucleophilic attack of the alcohol at the carbonyl of the intermediate. The involvement of a covalent intermediate, even though it may be cleaved differently (e.g., by attacking the saturated carbon), would most likely give a product which retains the absolute configuration and has already been ruled out (see above). In the case of cholesterol epoxide hydrolase, no ester intermediate could be identified (*71*). This enzyme appears to employ a mechanism fundamentally different from soluble and microsomal epoxide hydrolases (*71*) but possibly similar to the one proposed here involving a base-promoted nucleophilic attack of a water molecule.

One class of glycosidases catalyzing carbohydrate hydrolysis, with inversion of the anomeric configuration, is also mechanistically related to 5C8. Two carboxylic acid residues are normally present in the active site of these enzymes (Figure 8C), one of which is believed to act as an acid, protonating the glycosidic oxygen, while the other is thought to function as a base, promoting the attack of the nucleophile (*72*), equivalent to the supposed functions of Asp^{H95} and His^{L89} in 5C8. This similarity suggests that a mutation of His^{L89} to an aspartate or glutamate may also yield a catalyst for the ring closure reaction. Interestingly, no aspartic acid has so far been observed at position L89, and only 5 of over 2000 murine κ-light chain sequences contain a glutamate at that position (*72*). Thus, the chances seem low of eliciting such a mutant in mice by immunization with haptens **4** and **5**.

Conclusion. Antibodies 5C8, 14B9, 17F6, and 26D9 catalyze ring closure reactions that are strongly disfavored in solution. The observed catalytic effect is most likely due to an interplay between electronic stabilization and general acid/base catalysis. The fact that transition-state analogues **4** and **5** yield similar quality catalysts underlines the importance of charge stabilization for the catalysis of the disfavored reaction (*54*). In both cases, only parts of the stereoelectronic features of the transition state have been modeled into the hapten. Nevertheless, the combinatorial diversity of the immune system seems to be powerful enough and has, to some extent, been able to provide additional groups important for catalysis. The structural results suggest that further modifications of the transition-state analogue, which include replacing substituents of the piperidinium ring, and mutations in the active site may improve the efficiency of these catalytic antibodies.

ACKNOWLEDGMENT

We thank the Stanford Synchrotron Radiation Laboratory for data collection time and the staff of beamlines 7-1 and

9-1 for their assistance, P. A. Horton for technical assistance, A. Heine, M. Degano, and R. L. Stanfield for helpful discussions and comments, E. A. Stura for his help in crystallization, T. Jones and D. Kubitz for the antibody sequence determinations, J. Na for providing the coordinates of the original transition-state models, Q. Deng and B. Beno for their help in the quantum-chemical and modeling calculations, and K. Renner for computational assistance. This is manuscript No. 11299-MB from The Scripps Research Institute.

REFERENCES

1. Schultz, P. G., and Lerner, R. A. (1995) *Science 269*, 1835−1842.
2. Tramontano, A., Janda, K. D., and Lerner, R. A. (1986) *Science 234*, 1566−1570.
3. Pollack, S. J., Jacobs, J. W., and Schultz, P. G. (1986) *Science 234*, 1570−1573.
4. Thomas, N. R. (1996) *Nat. Prod. Rep. 13*, 479−511.
5. Haynes, M. R., Stura, E. A., Hilvert, D., and Wilson, I. A. (1994) *Science 263*, 646−652.
6. Zhou, G. W., Guo, J., Huang, W., Fletterick, R. J., and Scanlan, T. S. (1994) *Science 265*, 1059−1064.
7. Golinelli-Pimpaneau, B., Gigant, B., Bizebard, T., Navaza, J., Saludjian, P., Zemel, R., Tawfik, D. S., Eshhar, Z., Green, B. S., and Knossow, M. (1994) *Structure 2*, 175−183.
8. Charbonnier, J. B., Carpenter, E., Gigant, B., Golinelli-Pimpaneau, B., Eshhar, Z., Green, B. S., and Knossow, M. (1995) *Proc. Natl. Acad. Sci. U.S.A. 92*, 11721−11725.
9. Hsieh-Wilson, L. C., Schultz, P. G., and Stevens, R. G. (1996) *Proc. Natl. Acad. Sci. U.S.A. 93*, 5363−5367.
10. Patten, P. A., Gray, N. S., Yang, P. L., Marks, C. B., Wedemayer, G. J., Boniface, J. J., Stevens, R. C., and Schultz, P. G. (1996) *Science 271*, 1086−1091.
11. Wedemayer, G. J., Wang, L. H., Patten, P. A., Schultz, P. G., and Stevens, R. C. (1997) *J. Mol. Biol. 268*, 390−400.
12. Ulrich, H. D., Mundorff, E., Santarsiero, B. D., Driggers, E. M., Stevens, R. C., and Schultz, P. G. (1997) *Nature 389*, 271−275.
13. Charbonnier, J.-B., Golinelli-Pimpaneau, B., Gigant, B., Tawfik, D. S., Chap, R., Schindler, D. G., Kim, S.-H., Green, B. S., Eshhar, Z., and Knossow, M. (1997) *Science 275*, 1140−1142.
14. Barbas, C. F., Heine, A., Zhong, G., Hoffmann, T., Gramatikova, S., Björnstedt, R., List, B., Anderson, J., Stura, E. A., Wilson, I. A., and Lerner, R. A. (1997) *Science 278*, 2085−2092.
15. Heine, A., Stura, E. A., Yli-Kauhaluoma, J. T., Gao, C., Deng, Q., Beno, B. R., Houk, K. N., Janda, K. D., and Wilson, I. A. (1998) *Science 279*, 1934−1940.
16. Romesberg, F. E., Spiller, B., Schultz, P. G., and Stevens, R. C. (1998) *Science 279*, 1929−1933.
17. Janda, K. D., Shevlin, C. G., and Lerner, R. A. (1993) *Science 259*, 490−493.
18. Baldwin, J. E. (1976) *J. Chem. Soc., Chem. Commun.*, 734−736.
19. Baldwin, J. E., and Kruse, L. I. (1977) *J. Chem Soc., Chem. Commun.*, 233−235.
20. Gouverneur, V. E., Houk, K. N., de Pascual-Teresa, B., Beno, B., Janda, K. D., and Lerner, R. A. (1993) *Science 262*, 204−208.
21. Yli-Kauhaluoma, J. T., Ashley, J. A., Lo, C.-H., Tucker, L., Wolfe, M. M., and Janda, K. D. (1995) *J. Am. Chem. Soc. 117*, 7041−7047.
22. Cravatt, B. F., Ashley, J. A., Janda, K. D., Boger, D. L., and Lerner, R. A. (1994) *J. Am.Chem. Soc. 116*, 2261−2270.
23. Na, J., Houk, K. N., Shevlin, C. G., Janda, K. D., and Lerner, R. A. (1993) *J. Am. Chem. Soc. 115*, 8453−8454.
24. Janda, K. D., Shevlin, C. G., and Lerner, R. A. (1995) *J. Am. Chem. Soc. 117*, 2659−2660.
25. Sharpless, K. B., Amberg, W., Bennani, Y. L., Crispino, G. A., Hartung, J., Jeong, K.-S., Kwong, H. L., Morikawa, K., Wang, Z.-M., Xu, D., and Zhang, X.-L. (1992) *J. Org. Chem. 57*, 2768−2771.
26. Kolb, H. C., and Sharpless, K. B. (1992) *Tetrahedron 48*, 10515−10530.
27. Stura, E. A., Fieser, G. G., and Wilson, I. A. (1993) *ImmunoMethods 3*, 164−179.
28. Heine, A., Stefanko, R. S., Horton, P. A., Fieser, G. G., Gruber, K., Xu, J., Stura, E. A., and Wilson, I. A. (1999) (manuscript in preparation).
29. Otwinowski, Z., and Minor, W. (1997) *Methods Enzymol. 276*, 307−326.
30. Bailey, S. (1994) *Acta Crystallogr., Sect. D 50*, 760−763.
31. Navaza, J. (1994) *Acta Crystallogr., Sect. A 50*, 157−163.
32. Gruber, K., Heine, A., Stura, E. A., Lerner, R. A., Shevlin, C. G., and Wilson, I. A. (1999) (manuscript in preparation).
33. Brünger, A. T. (1992) *Nature 355*, 472−475.
34. Engh, R. A., and Huber, R. (1991) *Acta Crystallogr., Sect. A 47*, 392−400.
35. Read, R. J. (1986) *Acta Crystallogr., Sect. A 42*, 140−149.
36. McRee, D. E. (1993) in *Practical Protein Crystallography*, pp 273, Academic Press, Inc., San Diego, CA.
37. Bhat, T. N., and Cohen, G. H. (1984) *J. Appl. Crystallogr. 17*, 244−248.
38. Vellieux, F. M. D., and Dijkstra, B. W. (1997) *J. Appl. Crystallogr. 30*, 396−399.
39. Jones, T. A., Zou, J. Y., Cowan, S., and Kjeldgaard, M. (1991) *Acta Crystallogr., Sect. A 47*, 110−119.
40. Hodel, A., Kim, S.-H., and Brünger, A. T. (1992) *Acta Crystallogr., Sect. A 48*, 851−859.
41. Jiang, J.-S., and Brünger, A. T. (1994) *J. Mol. Biol. 243*, 100−115.
42. Kabat, E. A., Wu, T. T., Perry, H. M., Gottesmann, K. S., and Foeller, C. (1991) *Sequences of Proteins of Immunological Interest*, 5th ed., National Institutes of Health, Bethesda, MD.
43. Stanfield, R. L., Fieser, T. M., Lerner, R. A., and Wilson, I. A. (1990) *Science 248*, 712−719.
44. Thornton, J. M., MacArthur, M. W., McDonald, I. K., Jones, D. T., Mitchell, J. B. O., Nandi, C. L., Price, S. L., and Zvelebil, M. J. J. M. (1993) *Philos. Trans. R. Soc. London, Ser. A 345*, 113−129.
45. Arevalo, J. H., Stura, E. A., Taussig, M. J., and Wilson, I. A. (1993) *J. Mol. Biol. 231*, 103−118.
46. Dewar, M. J. S., Stewart, J. J. P., Zoebisch, E. G., and Healy, E. F. (1985) *J. Am. Chem. Soc. 107*, 3902−3909.
47. Goodsell, D. S., and Olson, A. J. (1990) *Proteins: Struct., Funct., Genet. 8*, 195−202.
48. Goodsell, D. S., Morris, G. M., and Olson, A. J. (1996) *J. Mol. Recognit. 9*, 1−5.
49. Connolly, M. L. (1983) *J. Appl. Crystallogr. 16*, 548−558.
50. Gelin, B. R., and Karplus, M. (1979) *Biochemistry 18*, 1256−1268.
51. Kohler, G., and Milstein, C. (1975) *Nature 256*, 495−497.
52. Engvall, E. (1980) *Methods Enzymol. 70*, 419−439.
53. Nicolaou, K. C., Prasad, C. V. C., Somers, P. K., and Hwang, C. K. (1989) *J. Am. Chem. Soc. 111*, 5330−5334.
54. Na, J., and Houk, K. N. (1996) *J. Am. Chem. Soc. 118*, 9204−9205.
55. Frisch, M. J., Trucks, G. W., Schlegel, H. B., Gill, P. M. W., Johnson, B. G., Robb, M. A., Cheeseman, J. R., Keith, T., Petersson, G. A., Montgomery, J. A., Raghavachari, K., Al-Laham, M. A., Zakrazewski, V. G., Ortiz, J. V., Foresman, J. B., Cioslowski, J., Stefanov, B. B., Nanayakkara, A., Challacombe, M., Peng, C. Y., Ayala, P. Y., Chen, W., Wong, M. W., Andres, J. L., Replogle, E. S., Gomperts, R., Martin, R. L., Fox, D. J., Binkley, J. S., Defrees, D. J., Baker, J., Stewart, J. P., Head-Gordon, M., Gonzales, C., and Pople, J. A. (1995) Gaussian, Inc., Pittsburgh, PA.
56. Amzel, L. M., and Poljak, R. J. (1979) *Annu. Rev. Biochem. 48*, 961−997.
57. Stanfield, R. L., and Wilson, I. A. (1998) in *Inflammation: Basic Principles and Clinincal Correlates* (Gallin, J. I., and Snyderman, R., Eds.) pp 267−279, Lippincott-Raven, Philadelphia, PA.

58. Chothia, C., Lesk, A. M., Tramontano, A., Levitt, M., Smith-Gill, S. J., Air, G., Sheriff, S., Padlan, E. A., Davies, D., Tulip, W. R., Colman, P. M., Spinelli, S., Alzari, P. M., and Poljak, R. J. (1989) *Nature 342*, 877−883.
59. Shalaby, M. R., Shepard, H. M., Presta, L., Rodrigues, M. L., Bevereley, P. C. L., Feldmann, M., and Carter, P. (1992) *J. Exp. Med. 175*, 217−225.
60. Johnson, G., Kabat, E. A., and Wu, T. T. (1995), National Center for Biotechnology Information, National Library of Medicine, National Insititutes of Health, Bethesta, MD.
61. Chou, H. N., and Shimizu, Y. (1987) *J. Am. Chem. Soc. 109*, 2184−2185.
62. Lee, M. S., Repeta, D. J., and Nakanishi, K. (1986) *J. Am. Chem. Soc. 108*, 7855−7856.
63. Krishna Prasad, A. V., and Shimizu, Y. (1989) *J. Am. Chem. Soc. 111*, 6476−6477.
64. Lee, M. S., Qin, G.-W., Nakanishi, K., and Zagorski, M. G. (1989) *J. Am. Chem. Soc. 111*, 6234−6241.
65. Townsend, C. A., and Basak, A. (1991) *Tetrahedron 47*, 2591−2602.
66. Holmes, D. S., Sherringham, J. A., Dyer, U. C., Russell, S. T., and Robinson, J. A. (1990) *Helv. Chim. Acta 73*, 239−259.
67. Evans, D. A., and DiMare, M. (1986) *J. Am. Chem. Soc. 108*, 2476−2478.
68. VanMiddlesworth, F., Patel, D. V., Donaubauer, J., Gannett, P., and Sih, C. J. (1985) *J. Am. Chem. Soc. 107*, 2996−2997.
69. Borhan, B., Jones, A. D., Pinot, F., Grant, D. F., Kurth, M. J., and Hammock, B. D. (1995) *J. Biol. Chem. 270*, 26923−26930.
70. Arand, M., Wagner, H., and Oesch, F. (1996) *J. Biol. Chem. 271*, 4223−4229.
71. Müller, F., Arand, M., Frank, H., Seidel, A., Hinz, W., Winkler, L., Hänel, K., Blee, E., Beetham, J. K., Hammock, B. D., and Oesch, F. (1997) *Eur. J. Biochem. 245*, 490−496.
72. McCarter, J. D., and Withers, S. G. (1994) *Curr. Opin. Struct. Biol. 4*, 885−892.
73. Kraulis, P. J. (1991) *J. Appl. Crystallogr. 24*, 946−950.
74. Bacon, D. J., and Anderson, W. F. (1988) *J. Mol. Graphics 6*, 219−220.
75. Merritt, E. A., and Murphy, M. E. P. (1994) *Acta Crystallogr., Sect. D 50*, 869−873.
76. Livingstone, C. D., and Barton, G. J. (1993) *Comput. Appl. Biosci. 9*, 745−756.
77. Thompson, J. D., Higgins, D. G., and Gibson, T. J. (1994) *Nucleic Acids Res. 22*, 4673−4680.
78. Barton, G. J. (1993) *Protein Eng. 6*, 37−40.

BI990210S